Quantum Spin Correlations in an Organometallic Alternating-Sign Chain

M. B. Stone,[1] W. Tian,[2,3] M. D. Lumsden,[1] G. E. Granroth,[1] D. Mandrus,[4] J.-H. Chung,[5,6] N. Harrison,[7] and S. E. Nagler[1]

[1]*Neutron Scattering Science Division, Oak Ridge National Laboratory, Oak Ridge, Tennessee 37831, USA*
[2]*Department of Physics and Astronomy, The University of Tennessee, Knoxville, Tennessee 37996, USA*
[3]*Ames Laboratory and Department of Physics and Astronomy, Iowa State University, Ames, Iowa 50011, USA*
[4]*Materials Science and Technology Division, Oak Ridge National Laboratory, Oak Ridge, Tennessee 37831, USA*
[5]*NCNR, National Institute of Standards and Technology, Gaithersburg, Maryland 20899, USA*
[6]*Department of Materials Science and Engineering, University of Maryland, College Park, Maryland 20742, USA*
[7]*National High Magnetic Field Laboratory, LANL, Los Alamos, New Mexico 87545, USA*

(Received 3 May 2007; published 24 August 2007)

High resolution neutron scattering is used to study excitations in the organometallic magnet $(CH_3)_2NH_2CuCl_3$ ($DMACuCl_3$). Combined with bulk magnetization and susceptibility studies, the new results imply that $DMACuCl_3$ is a realization of the $S = 1/2$ alternating antiferromagnetic-ferromagnetic (AFM-FM) chain. Coupled-cluster calculations indicate that the AFM and FM interactions have nearly the same strength, while analysis of scattering intensities shows evidence for interdimer spin correlations. Results are discussed in the context of recent ideas concerning quantum entanglement.

DOI: 10.1103/PhysRevLett.99.087204 PACS numbers: 75.10.Pq, 75.10.Jm, 75.30.Et, 75.40.Gb

Low dimensional, dimerized quantum spin systems exhibit diverse physics ranging from simple spin gaps to exotic spin liquids [1–4]. A prototypical example is the $S = 1/2$ Heisenberg alternating chain (HAC), defined by the Hamiltonian $\mathcal{H} = \sum_n J_1 \mathbf{S}_{2n-1} \cdot \mathbf{S}_{2n} + J_2 \mathbf{S}_{2n} \cdot \mathbf{S}_{2n+1}$. The HAC has been widely studied theoretically [5–7] and experimentally [8]. Considering $J_1 > 0$ antiferromagnetic (AFM), ground state behavior of the HAC depends on the ratio $\alpha = J_2/J_1$. $\alpha = 1$ corresponds to the quantum critical pure AFM chain. When $|\alpha| \ll 1$ the system behaves as nearly independent dimers, and perturbation theory in α provides a straightforward approach to calculate physical properties of the spin gap system. For $\alpha < 0$, one has a realization of the antiferromagnetic-ferromagnetic (AFM-FM) HAC. For $\alpha \ll -1$, the HAC maps onto the $S = 1$ AFM Haldane chain with the spin viewed as a composite object [9–11]. The regime $\alpha \approx -1$ is particularly interesting since the system exhibits intermediate behavior between dimer and Haldane physics [9,12]. Calculating physical properties must be done carefully since perturbation theory from the dimer limit is not a good approximation here.

We report new inelastic neutron scattering (INS) results for $(CH_3)_2NH_2CuCl_3$ ($DMACuCl_3$ or MCCL). We use state of the art linked-cluster calculations [11,13] and bulk measurements to show $DMACuCl_3$ contains a realization of the AFM-FM HAC with $\alpha = -0.92(4)$. Moreover, in contrast to results on existing AFM-AFM HACs [8], there is evidence for spatially extended entanglement of the principle dimers via the FM coupled spins.

$DMACuCl_3$ is monoclinic with $\beta = 97.5°$ at room temperature with Cu-Cl planes separated along c by methyl groups, i.e., magnetic coupling is only expected in the ab plane as shown in Fig. 1 [14]. Thermodynamic and structural considerations suggested that $DMACuCl_3$ was an AFM-FM HAC along the a axis with $\alpha \approx -1$ [15–17], attracting interest since other experimental realizations of AFM-FM HACs have $\alpha \ll -1$ [18,19]. Further measurements were interpreted as independent FM and AFM dimers with evidence for a transition to long range order below $T = 0.9$ K [20,21]. Preliminary INS in the disordered phase eliminated both independent dimer and a-axis chain models [22]. Recently, it was shown that the low-temperature (LT), $T < 285$ K, structure is triclinic with two independent chains along the high-temperature (HT) b axis [23,24], cf. Fig. 1. Bond lengths in the LT structure favor HAC Cu-Cl-Cl-Cu or Cu-Cl-Cu exchange paths, found to be relevant in other low-dimensional magnets [2–4].

Deuterated samples were obtained by slow evaporation of D_2O solutions of $CuCl_2$ and $(CD_3)_2ND \cdot HCl$. A 2.23 g

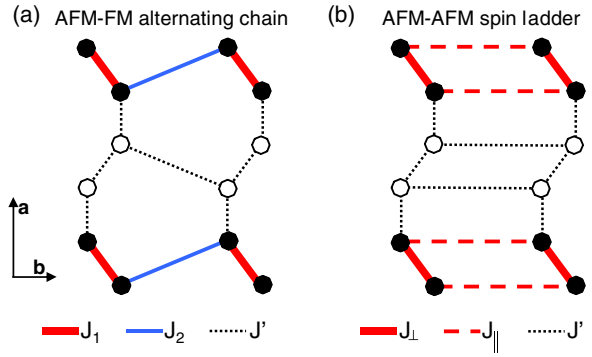

FIG. 1 (color online). Cu^{2+} $S = 1/2$ sites in an ab plane of $DMACuCl_3$. ○ and ● illustrate two distinct dimer bonds/chains in the LT phase[24]. (a) AFM-FM HAC scenario with J_1 and J_2 shown as solid lines and weaker exchange, J', shown as dotted lines. (b) AFM-AFM SL scenario with $J_\perp$ and $J_\parallel$. Lattice vectors correspond to HT monoclinic parameters [14].

single crystal mounted in the $(hk0)$ plane was examined using the SPINS spectrometer at NIST configured with 80′ collimation before and after the sample and a cold Be filter in the scattered beam. A flat PG(002) analyzer selected scattered neutrons at 5 meV. Constant wave-vector, $\mathbf{Q}$, scans were performed at $T = 1.8$ K indexing $\mathbf{Q}$ in the HT monoclinic notation with LT lattice constants, $a = 12.05$ Å and $b = 8.43$ Å [14].

Representative constant-$\mathbf{Q}$ scans are shown in Fig. 2. A single excitation disperses along k between $0.95(2) \leq \hbar\omega \leq 1.66(2)$ meV as shown in Fig. 2(a)–2(d). The mode is only weakly dispersive along h at the bottom [Fig. 2(e) and 2(f)] and top [Fig. 2(g) and 2(h)] of the band with $\approx 0.2(1)$ meV dispersion along (h 1.5 0). Intensity reduction for temperatures large compared to the energy scales of excitations indicates their magnetic origin, cf. Fig. 2(c). The intrinsic peak width is small compared to the instrumental resolution of ≈ 0.25 meV FWHM. We find no significant evidence for gapless excitations or magnetic continuum scattering.

We fit the constant-$\mathbf{Q}$ scans with Gaussian peaks to determine dispersion and intensity variation in the $(hk0)$ plane as summarized in Fig. 3. Lack of dispersion along h excludes the proposed a axis as the chain axis, and significant dispersion along k excludes noninteracting dimer models. The k dispersion has periodicity 2π in reduced units, a quantum effect showing a lack of AFM order. The FM-FM HAC is ruled out by the absence of a second dispersive mode [25]. Notably, the band maximum (minimum) is at $Q = 2m\pi[(2m + 1)\pi]$ for integer m. This is unusual and rules out a HAC with $\alpha > 0$. Models that can produce such dispersion include the AFM-FM HAC and the AFM-AFM spin ladder (SL) with the HAC favored due to structural arguments.

The dispersion for the HAC and SL models can be calculated using perturbation theory to first order, $\hbar\omega(\mathbf{Q}) = \epsilon_1 + \epsilon_2 \cos(\mathbf{Q} \cdot \mathbf{u})$ [5,7,9,26], where $\epsilon_1 = J_1(J_\perp)$ and $\epsilon_2 = \frac{|J_2|}{2}(J_\parallel)$ for the HAC (SL) models with the interdimer vector $\mathbf{u}$. It is more accurate to use state of the art linked-cluster-expansion methods [11,13]. Parameters obtained from fits of the data to these models are summarized in Table I. Perturbation theory is clearly inadequate to describe the AFM-FM HAC as evidenced by the large difference in fitting parameters relative to the linked-cluster method. Dispersion alone cannot differentiate between the HAC and SL models, cf. Fig. 3(a).

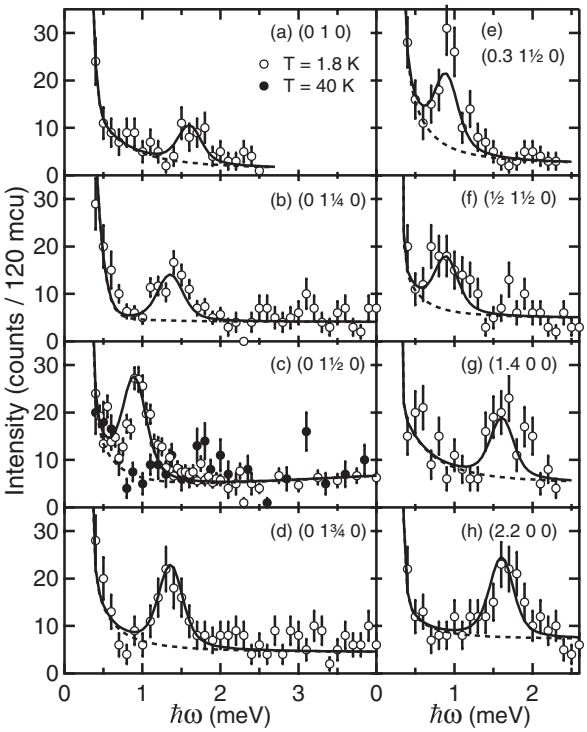

FIG. 2. $T = 1.8$ K constant-$\mathbf{Q}$ scans of $DMACuCl_3$. (c) includes data at $T = 40$ K. Lines are based upon a global fit to the AFM-FM HAC model described in the text. Dashed lines are fitted backgrounds. Intensity is normalized to incident neutron flux with 120 m.c.u. (monitor count units) corresponding to ≈ 2 minutes.

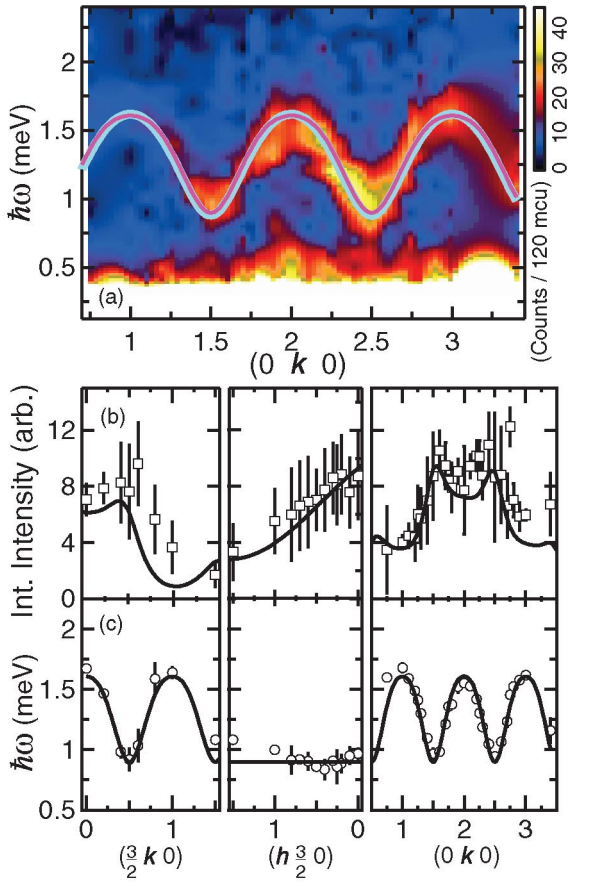

FIG. 3 (color). (a) Scattering intensity vs $\hbar\omega$ along $(0k0)$. Solid lines are fits to linked-cluster model dispersions, AFM-FM HAC (cyan) and AFM-AFM SL (magenta). (b) Integrated intensity vs $\mathbf{Q}$. Error bars include error in fitted background, cf. Fig. 2. (c) Dispersion based upon Gaussian peak approximation. Lines in (b) and (c) are based upon a global fit to the AFM-FM HAC model described in the text.

TABLE I. Fitted dispersion parameters for AFM-FM HAC and AFM-AFM SL models using linked-cluster expansions (E) and perturbation theory (PT).

Model (method)	J_1 or $J_\perp$ (meV)	J_2 or $J_\parallel$ (meV)
AFM-FM HAC (E)	1.406(8)	−1.30(5)
AFM-FM HAC (PT)	1.319(8)	−0.68(2)
AFM-AFM SL (E)	1.194(6)	0.376(5)
AFM-AFM SL (PT)	1.319(8)	0.34(1)

In principle, high field INS can differentiate the SL and HAC models [27]. A definitive measurement for $DMACuCl_3$ would require magnetic fields over 20 T, not available presently. In zero field, the wave-vector dependent INS intensity could also be used to differentiate these models, but because of the specific geometry of the bonding in the compound, these differences are very minor. However, careful analysis of bulk field dependent thermodynamic measurements along with the zero field INS data allows additional differentiation between the two models. Figure 4(a) shows pulsed field magnetization of $DMACuCl_3$ up to 20 T at $T = 1.6$ K. The upper critical field where all spins are FM aligned is in the vicinity of 16 T. We also plot quantum Monte Carlo (QMC) calculations [28] of the magnetization for 100 spins using exchange constants determined from cluster-expansion fits of $\hbar\omega(\mathbf{Q})$. The AFM-FM HAC model better reproduces the upper critical field, but neither model alone accounts for the linear magnetization at low field.

Recall that the LT structure has two types of bonding, i.e., two sets of exchange parameters for quasi-1D chains

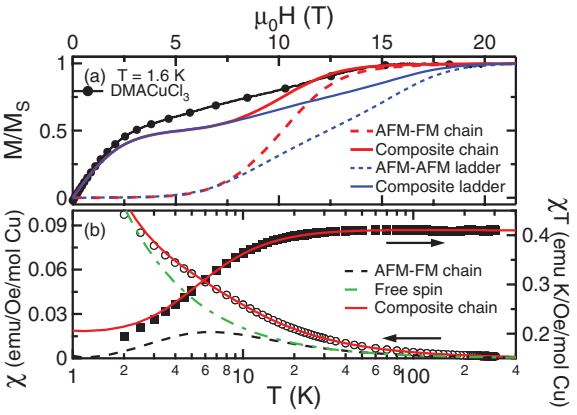

FIG. 4 (color). (a) Pulsed field magnetization of $DMACuCl_3$ powder at $T = 1.6$ K. Lines are QMC calculations based upon AFM-FM HAC and AFM-AFM SL models. Solid lines, labeled as composite chain or composite ladder, include a free-spin contribution. Symbols for data are plotted every 1000 points. (b) Single crystal magnetic susceptibility, $\chi(T)$, and $\chi(T)T$ for $\mu_0 H = 0.05$ T with $H \parallel a$. Lines are the composite model AFM-FM HAC polynomial fit discussed in the text. Broken lines are the $\chi(T)$ contribution of the AFM-FM HAC (dashed black) and free-spin (dash-dot green) components of the composite model.

along the monoclinic b axis. There is no evidence for a higher energy mode in either INS or thermodynamic measurements. The present experiment therefore sets an upper limit of $J' \approx 0.2$ meV for the energy scale associated with a second chain, indistinguishable from the incoherent elastic scattering. To account for the second chain, we calculate $M(H)$ as a composite model with half the moments included as free spins. A conjecture of a free-spin contribution was also made in Ref. [29]. As seen in Fig. 4(a), the composite AFM-FM HAC model calculation is a much better description of the measurement than the composite AFM-AFM SL model, accounting for both the low-field and high-field limits. Deviations from the data in the vicinity of 5 to 10 T may be a consequence of a field-induced collective ordered phase [21] that is not accounted for in the calculation. Willet *et al.* use finite chain calculations to obtain parameters that reproduce $M(H)$ favoring a two chain model[24]. However, the exchange parameters they propose are incompatible with the measured dispersion.

Temperature dependent magnetic susceptibility, $\chi(T)$, also agrees with the AFM-FM HAC:free-spin composite model. The solid lines in Fig. 4(b) are a fit using the composite model, with $\chi(T)$ for the HAC calculated using a polynomial representation derived from finite-sized scaling [19]. The parameters $J_1 = 0.973(4)$, $J_2 = -1.23(5)$ meV, and $g = 2.096(1)$ are reasonably consistent with INS results although the latter provides a more direct measure of the exchange parameters. We therefore conclude that MCCL contains an AFM-FM HAC with the most reliable estimate of $\alpha = -0.92(4)$ obtained from the fit of the INS dispersion to the cluster-expansion model.

The wave-vector dependence of the neutron scattering intensity reflects the underlying geometry of the system and can be used to determine whether the AFM bond, J_1, is the short or long bond in $DMACuCl_3$ (cf. Fig. 1). The intensities for a straight chain can be calculated directly using the coupled cluster-expansion method; however, this does not account for the complicated zigzag geometry and out of plane displacements present in $DMACuCl_3$. To include the complete geometry we use a single mode approximation (SMA) to calculate the dynamical correlation function. The SMA is justified by the observation that the INS data show a single peak with no appreciable additional intensity, and that the calculated spectral weight is dominated by single particle excitations for $\alpha \approx -1$ [11]. The SMA to the scattering intensity is

$$\tilde{I}_m(\mathbf{Q},\hbar\omega) \propto -\frac{|F(Q)|^2}{\hbar\omega(\mathbf{Q})}\sum_{\mathbf{d}} J_{\mathbf{d}}\langle \mathbf{S}_0\cdot\mathbf{S}_{\mathbf{d}}\rangle[1-\cos(\mathbf{Q}\cdot\mathbf{d})] \times \delta(\hbar\omega-\hbar\omega(\mathbf{Q})). \quad (1)$$

$\langle \mathbf{S}_0\cdot\mathbf{S}_{\mathbf{d}}\rangle$ is the two spin correlation function [30]. The sum over the bond vectors $\mathbf{d}$ is restricted to two terms: the AFM bond $\mathbf{d}_1$ and the FM bond $\mathbf{d}_2$. The dispersion of the mode is derived from the cluster-expansion expression for the AFM-FM HAC. The SMA is compared to the data by a

global fit of Eq. (1) convolved with the instrumental resolution to 74 constant-**Q** scans. Fitting parameters include an overall scaling factor and the ratio $A = \alpha \frac{\langle \mathbf{S}_0 \cdot \mathbf{S}_{\mathbf{d}_2} \rangle}{\langle \mathbf{S}_0 \cdot \mathbf{S}_{\mathbf{d}_1} \rangle}$. The exchange constants are fixed at the best-fit values of Table I with $\alpha = -0.92(4)$. With the choice of the short AFM bond, the results reproduce both the dispersion and the observed intensity modulation very well and are shown as solid lines in Figs. 2, 3(b), and 3(c), with $A = 0.26(4)$. Choosing the long AFM bond results in an inferior fit. This result is consistent with the conclusions of Willett *et al.* based upon structural arguments. If one allows the exchange constants to vary the resulting global fit parameters are $J_1 = 1.399(6)$ and $J_2 = -1.07(3)$ meV, and $A = 0.27(4)$ with $\alpha = -0.76(4)$.

The nonzero value of the ratio A shows a fundamental difference between the AFM-FM HAC and the AFM-AFM HAC; for the latter empirically $A = 0$ [8]. The physical meaning of this may be related to the spatial extent of quantum entanglement in the system. Recent work discusses how the degree of entanglement is directly related to spin correlations such as those measured in neutron scattering experiments [31–33]. Brukner *et al.* show specifically how this applies to the AFM-AFM HAC, and, in particular, that the correlation $\langle \mathbf{S}_0 \cdot \mathbf{S}_{\mathbf{d}1} \rangle$ determined by fits to the SMA acts as an entanglement witness, with $|\langle \mathbf{S}_0 \cdot \mathbf{S}_{\mathbf{d}_r} \rangle|$ greater than the classical limit $\frac{1}{4}$ implying that quantum entanglement is significant. At low temperatures, experimental realizations of the AFM-AFM HAC have $\langle \mathbf{S}_0 \cdot \mathbf{S}_{\mathbf{d}1} \rangle$ consistent with the fully entangled isolated dimer value of $-\frac{3}{4}$, while $\langle \mathbf{S}_0 \cdot \mathbf{S}_{\mathbf{d}2} \rangle = 0$, implying that AFM dimers are not mutually entangled. In contrast, the present results show that $\langle \mathbf{S}_0 \cdot \mathbf{S}_{\mathbf{d}2} \rangle$ is nonzero. Although it is not possible to independently extract the values of $\langle \mathbf{S}_0 \cdot \mathbf{S}_{\mathbf{d}1} \rangle$ and $\langle \mathbf{S}_0 \cdot \mathbf{S}_{\mathbf{d}2} \rangle$, the results strongly suggest that the spatial extent of entanglement is greater for the AFM-FM chain. Indeed for $\alpha = -\infty$ the FM dimer evolves to a composite spin $S = 1$ entity [34], with an expectation of $T = 0$ correlations extending over several lattice spacings. The AFM-FM HAC may serve as an excellent model system for studying the spatial evolution of quantum entanglement

In summary, high resolution INS, combined with high field magnetization and magnetic susceptibility measurements show that $DMACuCl_3$ is a quasi-1D AFM-FM HAC with $\alpha \approx -1$, intermediate between weakly coupled dimer and Haldane regimes. The exchange parameters are determined from the dispersion using the results of coupled-cluster series expansions. Applying the SMA to analyze the scattering intensity suggests that interdimer spin entanglement is significant in $DMACuCl_3$ in contrast to previously studied AFM-AFM HACs.

We acknowledge discussions with M. Meisel, A. Zheludev, T. Barnes, R. R. P. Singh, and W. Zheng. D. M. acknowledges B. Lake for drawing his attention to $DMACuCl_3$. Research sponsored by the Division of Materials Sciences and Engineering, Office of Basic Energy Sciences, US Department of Energy, under Contract No. DE-AC05-00OR22725 with Oak Ridge National Laboratory, managed and operated by UT-Battelle, LLC. This work utilized facilities supported in part by the National Science Foundation under Agreement No. DMR-0454672. The NHMFL is supported by the DOE, NSF, and Florida State University.

[1] D. Poilblanc *et al.*, Phys. Rev. B **73**, 100403(R) (2006).
[2] M. B. Stone *et al.*, Phys. Rev. B **64**, 144405 (2001).
[3] T. Masuda *et al.*, Phys. Rev. Lett. **96**, 047210 (2006).
[4] M. M. Turnbull *et al.*, Coord. Chem. Rev. **249**, 2567 (2005).
[5] A. Brooks Harris, Phys. Rev. B **7**, 3166 (1973).
[6] G. S. Uhrig and H. J. Schulz, Phys. Rev. B **54**, R9624 (1996).
[7] T. Barnes *et al.*, Phys. Rev. B **59**, 11 384 (1999).
[8] A. W. Garrett *et al.*, Phys. Rev. Lett. **79**, 745 (1997); B. Lake *et al.*, J. Phys. Condens. Matter **9**, 10 951 (1997); G. Xu *et al.*, Phys. Rev. Lett. **84**, 4465 (2000).
[9] K. Hida, Phys. Rev. B **45**, 2207 (1992); J. Phys. Soc. Jpn. **63**, 2514 (1994).
[10] S. Watanabe and H. Yokoyama, J. Phys. Soc. Jpn. **68**, 2073 (1999).
[11] W. Zheng *et al.*, Phys. Rev. B **74**, 172407 (2006).
[12] K. Hida, J. Phys. Soc. Jpn. **67**, 1416 (1998); M. Bocquet and Th. Jolicœur, Eur. Phys. J. B **14**, 47 (2000).
[13] J. Oitmaa *et al.*, Phys. Rev. B **54**, 1009 (1996); C. J. Hamer *et al.*, Phys. Rev. B **68**, 214408 (2003).
[14] R. Willet, J. Chem. Phys. **44**, 39 (1966).
[15] B. C. Gerstein *et al.*, J. Appl. Phys. **43**, 1932 (1972).
[16] M. Hurley and B. C. Gerstein, J. Chem. Phys. **59**, 6667 (1973).
[17] S. O'Brien *et al.*, Inorganica Chimica Acta **141**, 83 (1988).
[18] T. Nishikawa *et al.*, J. Phys. Soc. Jpn. **67**, 1988 (1998); M. Hagiwara *et al.*, J. Phys. Soc. Jpn. **66**, 1792 (1997); I. Vasilevesky *et al.*, Inorg. Chem. **30**, 4082 (1991).
[19] J. J. Borrás-Almenar *et al.*, Inorg. Chem. **33**, 5171 (1994).
[20] Y. Ajiro *et al.*, Physica (Amsterdam) **329–333B**, 1008 (2003).
[21] M. B. Stone *et al.*, AIP Conf. Proc. **850**, 1015 (2006).
[22] M. B. Stone *et al.*, Physica (Amsterdam) **385–386B**, 438 (2006).
[23] Y. Inagaki *et al.*, J. Phys. Soc. Jpn. **74**, 2683 (2005).
[24] R. D. Willett *et al.*, Inorg. Chem. **45**, 7689 (2006).
[25] G. Huang *et al.*, Phys. Rev. B **43**, 11 197 (1991).
[26] T. Barnes *et al.*, Phys. Rev. B **47**, 3196 (1993).
[27] R. Coldea *et al.*, Phys. Rev. Lett. **88**, 137203 (2002).
[28] http://alps.comp-phys.org/; M. Troyer *et al.*, Lect. Notes Comput. Sci. **1505**, 191 (1998).
[29] B. C. Watson, Ph.D. thesis, University of Florida, 2000.
[30] P. C. Hohenberg and W. Brinkman, Phys. Rev. B **10**, 128 (1974).
[31] F. Verstraete *et al.*, Phys. Rev. Lett. **92**, 027901 (2004).
[32] B.-Q. Jin and V. E. Korepin, Phys. Rev. A **69**, 062314 (2004).
[33] C. Brukner *et al.*, Phys. Rev. A **73**, 012110 (2006).
[34] See, e.g., S. Ma *et al.*, Phys. Rev. Lett. **69**, 3571 (1992); L. P. Regnault *et al.*, Phys. Rev. B **50**, 9174 (1994).